International Journal of Automation and Computing 14(2), April 2017, 179-190
DOI: 10.1007/s11633-016-1023-1

Quasi-inverse Pendulum Model of 12 DoF Bipedal Walking

M. Akhtaruzzaman Amir A. Shafie Md. Raisuddin Khan
Department of Mechatronics Engineering, Kulliyyah of Engineering, International Islamic University Malaysia, Kuala Lumpur 53100, Malaysia

Abstract: This paper presents modeling of a 12-degree of freedom (DoF) bipedal robot, focusing on the lower limbs of the system, and trajectory design for walking on straight path. Gait trajectories are designed by modeling of center of mass (CoM) trajectory and swing foot ankle trajectory based on stance foot ankle. The dynamic equations of motion of the bipedal robot are derived by considering the system as a quasi inverted pendulum (QIP) model. The direction and acceleration of CoM movement of the QIP model is determined by the position of CoM relative to the centre of pressure (CoP). To determine heel-contact and toe-off, two custom designed switches are attached with heel and toe positions of each foot. Four force sensitive resistor (FSR) sensors are also placed at the plantar surface to measure pressure that is induced on each foot while walking which leads to the calculation of CoP trajectory. The paper also describes forward kinematic (FK) and inverse kinematic (IK) investigations of the biped model where Denavit-Hartenberg (D-H) representation and Geometric-Trigonometric (G-T) formulation approach are applied. Experiments are carried out to ensure the reliability of the proposed model where the links of the bipedal system follow the best possible trajectories while walking on straight path.

Keywords: Humanoid robot, quasi-inverse pendulum, gait, trajectory planning, Anthropoid.

1 Introduction

Relating to the various configuration of joints and links of a humanoid robot, a specific set of equations establishes the association of end frame with reference frame. For the simplification of process, the position and orientation issues should be analyzed independently and need to be accumulated for the complete set of interrelated equations[1−3]. As the solution of inverse kinematic (IK) formulation, the necessary values for joint and link variables are required to identify to move the end point at expected locations with proper orientations. One of the simplest technique is geometric-trigonometric formulation where the valuated joint and link variables are accumulated into a tabulated form, known as mapping[4, 5].

In a real system, the suitable sequence of transformation depends on robot′s structure and its joint configurations[6, 7]. In Nao Humanoid, Hip pitch-yaw joints are designed using single servo which made the system distinguishable in presenting kinematics and movement patterns[8, 9]. Denavit-Hartenberg (D-H) representation strategy is applied as the solution of forward kinematic (FK) formulation, while IK solution is proposed with analytical approach that eliminates assumptions and singularities of its earlier models[10]. A different kinematic structure is reflected in SILO2 humanoid where FK analysis is performed utilizing screw theory to express product of exponentials formula (PoEF)[11, 12]. As a non-negligible offset exists at hip joint of SILO2, a hybrid mechanism is proposed for IK analysis. In this approach, geometric analytical solution is identified as the initial condition of numerical method to reduce the number of iteration[11].

Homogeneous coordinate transformation matrix is used by Lope et al.[13], to describe the position and orientation of foot. Kinematic structure of the system reflects PINO humanoid where IK solution is formulated based on artificial neural network (ANN) using two layered back propagation architecture. Zorjan and Hugel[14] presents a modified D-H convention, called DHKK. They applied geometric formulation only for knee joint and decomposed to calculate hip and ankle joint angles which allow the elimination of IK singularity[14]. Direct kinematic analysis using D-H strategy and geometric formulation are also reflected in a small sized biped called Ro-bonova-I[15]. Beside these, a biped with flexible ankle and split-mass balancing strategy has achieved stable walking by decoupling walking motion from sideway balancing control[16].

Many of the experimentations reflect flat-lifting and flat-landing (FL-FL) strategy for bipedal walking, while natural walking shows hill-contact and toe-off (HC-TO) pattern which is adopted in this study. Moreover, the leg swing motion is defined as a function of center of mass (CoM) to have lateral stability where co-relation between motion trajectories and acceleration is established through quasi-inverse pendulum (QIP) model of 12 DoF bipedal platform. Although, Section 2.3 presents a 14 DoF model (consider-

Research Article
Manuscript received December 14, 2014; accepted February 23, 2016; published online January 18, 2017
This works was supported by Ministry of Higher Education, Malaysia through the MyRA Incentive Grant Scheme (No. MIRGS 13-02-001-0001).
Recommended by Associate Editor Hong-Nian Yu
© Institute of Automation, Chinese Academy of Sciences and Springer-Verlag Berlin Heidelberg 2017

ing lower extremity), both of the toe joints are considered as fixed ($\theta_i = \theta_{13} = 0°$) for experimentation, as the biped has 12 DoF at lower kinematic chains.

The rest of the paper is organized as: Section 2 presents methodology of designing the walking model through identification of anatomical center of mass, calculation of moment of inertia, investigation of FK, formulation of walking stability, trajectory planning, and IK investigation. Section 3 presents sensor attachments and strategy in calculating CoP trajectory. Section 4 explains the designed algorithm and experimental results. Finally, concluding remarks are presented in Section 5. This research is the motivation of previous works which can be found in the reference section[17−25].

2 System analysis and design

2.1 Investigating anatomical CoM

Though CoM of a humanoid system shows dynamic behavior, the variations of the CoM positions are comparatively smaller for walking gait. Considering this factor, the CoM of the body is calculated using balance board technique, as presented in Fig. 1[26]. Here, L and m_1 are indicating length and CoM of the balance board, ($l_1 = l_2$). Humanoid body height and mass are indicated by H and m_2 (acting on the CoM point of body). Therefore, total mass ($m_1 + m_2$) of the entire setup is acting on the pivot point which is indicated by the distance x_1 from the center line of balance board. Pivot point is the critical point at which the board can balance itself parallel with ground. Distance of the CoM of body is considered as x_2 from the pivot point. In this setup, only x_2 remains unknown which is needed to be determined. Now, taking moments about the pivot point, x_2 can be calculated using the equation, presented in (1).

$$x_2 = \frac{(m_1 x_1)}{m_2}. \tag{1}$$

So, the height (h), of CoM point of the humanoid system can be calculated as

$$h = (H - l_1) + (x_1 + x_2). \tag{2}$$

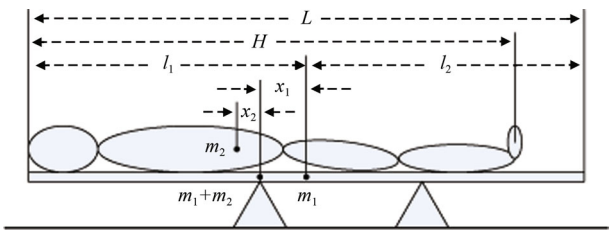

Fig. 1 Balance board strategy to calculate CoM of anatomical body

2.2 Investigating moment of Inertia (I)

Considering the human model as a complex pendulum, experimental setup has been made to calculate the period of oscillation, T, for sagittal plane and coronal plane. Axis of oscillation is considered at the ankle joint. Distance between ankle joint and foot of the humanoid system is measured as 3.3 cm. So, the height of CoM is considered from the ankle joint, ($h_{ank-CoM}$). For small angle, about 4°, T is calculated as follows by taking the average of 20 oscillations.

$$\begin{cases} T_{\text{sagittal}} = 0.937\,8\,\text{s} \\ T_{\text{coronal}} = 0.981\,35\,\text{s}. \end{cases} \tag{3}$$

The moment of inertia, I, is calculated based on (4) where M is the total mass of the humanoid, g is gravitational acceleration, $h_{ank-CoM}$ is the height of the CoM from the ankle joint and T is oscillation time of the humanoid compound pendulum. Moment of inertia for sagittal and coronal plane, I_S and I_C, are presented in (5).

$$I = Mgh_{ank-CoM}\left(\frac{T}{2\pi}\right)^2 \tag{4}$$

$$\begin{cases} I_S = 658\,717.345\,7\ \text{gm} \cdot \text{cm}^2 \\ I_C = 721\,317.546\ \text{gm} \cdot \text{cm}^2. \end{cases} \tag{5}$$

2.3 Forward kinematics (FK) investigation

For this experiment, humanoid multi-link composite platform is considered as five kinematic-chains connected at a common point, the hip joint, where CoM is considered for this experiment. The frame assignments for each joint are presented in Figs. 2 and 3.

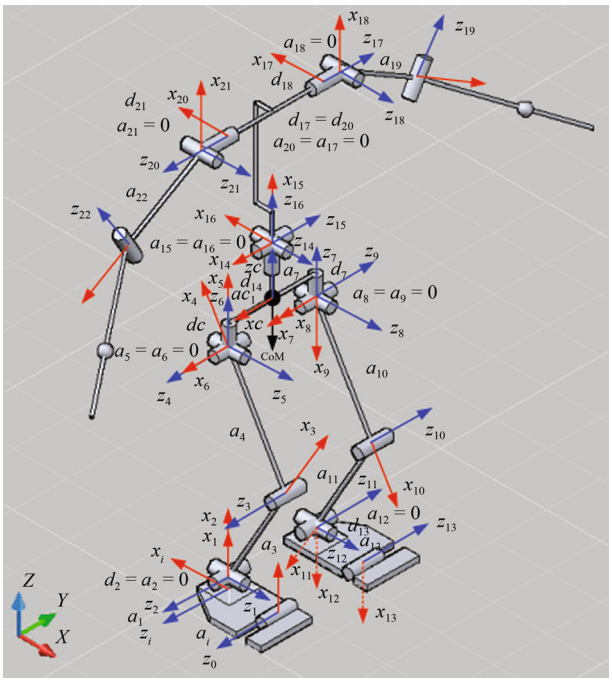

Fig. 2 Assigning the local frames to each joint considering the right-foot as base

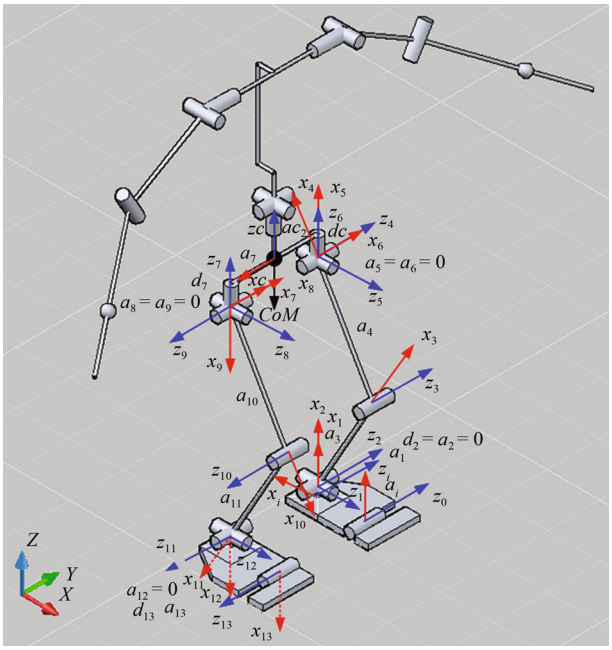

Fig. 3 Assigning the local frames to each joint considering the left-foot as base

To perform locomotion, humanoid robot always shifts its foot contact from left to right and vice versa, during double support phase (DSP). During single support phase (SSP), only one foot is in contact with ground. Focusing on the lower limbs, FK investigation is conducted for four configurations, right-foot to CoM, CoM to left-foot, left-foot to CoM, and CoM to right-foot. Tables 1 to 4 are presenting D-H parameters of lower kinematic chains of the model, where $\theta_i = \theta_{13} = 0^\circ$ is considered to make the model applicable for 12 DoF system.

Based on the D-H parameter tables, several A matrices are derived which are post multiplied to find out the general equations (T matrices) for forward kinematics of the chains. Equations (6)–(9) are presenting the T matrices.

Table 1 D-H parameters for right-toe base to CoM (${}^{RB}T_{CoM}$)

Joint axes	D-H parameters (${}^{RB}T_{CoM}$)			
	θ_n	d_n	a_n	α_n
i	$\theta_i = 0$	0	$a_i = L_2$	0
1	$\theta_1 = \frac{\pi}{2}$	0	$a_1 = L_3$	$\alpha_1 = \frac{\pi}{2}$
2	θ_2	0	0	$\alpha_2 = -\frac{\pi}{2}$
3	θ_3	0	$a_3 = L_4$	0
4	θ_4	0	$a_4 = L_5$	0
5	θ_5	0	0	$\alpha_5 = \frac{\pi}{2}$
6	θ_6	0	0	$\alpha_6 = \frac{\pi}{2}$
CoM	θ_C	$d_c = L_6$	$a_c = -L_7$	0

Table 2 D-H parameters for swinging leg, CoM to left-toe (${}^{CoM}T_{LS}$)

Joint axes	D-H parameters (${}^{CoM}T_{LS}$)			
	θ_n	d_n	a_n	α_n
7	0	$d_7 = -L_9$	$a_7 = -L_8$	0
8	θ_8	0	0	$\alpha_8 = -\frac{\pi}{2}$
9	θ_9	0	0	$\alpha_9 = -\frac{\pi}{2}$
10	θ_{10}	0	$a_{10} = L_{10}$	0
11	θ_{11}	0	$a_{11} = L_{11}$	0
12	θ_{12}	0	0	$\alpha_{12} = \frac{\pi}{2}$
13	$\theta_{13} = 0$	$d_{13} = L_{13}$	$a_{13} = L_{12}$	$\alpha_{13} = -\frac{\pi}{2}$

Table 3 D-H parameters for left-toe base to CoM (${}^{LB}T_{CoM}$)

Joint axes	D-H parameters (${}^{LB}T_{CoM}$)			
	θ_n	d_n	a_n	α_n
i	$\theta_i = 0$	0	$a_i = L_{13}$	0
1	$\theta_1 = \frac{\pi}{2}$	0	$a_1 = L_{12}$	$\alpha_1 = -\frac{\pi}{2}$
2	θ_2	0	0	$\alpha_2 = \frac{\pi}{2}$
3	θ_3	0	$a_3 = L_{11}$	0
4	θ_4	0	$a_4 = L_{10}$	0
5	θ_5	0	0	$\alpha_5 = -\frac{\pi}{2}$
6	θ_6	0	0	$\alpha_6 = -\frac{\pi}{2}$
CoM	θ_C	$d_c = L_9$	$a_c = -L_8$	0

Table 4 D-H parameters for swing leg, CoM to right-toe (${}^{CoM}T_{RS}$)

Joint axes	D-H parameters (${}^{CoM}T_{RS}$)			
	θ_n	d_n	a_n	α_n
7	0	$d_7 = -L_6$	$a_7 = -L_7$	0
8	θ_8	0	0	$\alpha_8 = \frac{\pi}{2}$
9	θ_9	0	0	$\alpha_9 = \frac{\pi}{2}$
10	θ_{10}	0	$a_{10} = L_5$	0
11	θ_{11}	0	$a_{11} = L_4$	0
12	θ_{12}	0	0	$\alpha_{12} = -\frac{\pi}{2}$
13	$\theta_{13} = 0$	$d_{13} = L_2$	$a_{13} = L_3$	$\alpha_{13} = \frac{\pi}{2}$

$$
{}^{RB}T_{CoM} = A_i A_1 A_2 A_3 A_4 A_5 A_6 A_{CoM} =
\begin{bmatrix}
n_{x(RBC)} & o_{x(RBC)} & a_{x(RBC)} & p_{x(RBC)} \\
n_{y(RBC)} & o_{y(RBC)} & a_{y(RBC)} & p_{y(RBC)} \\
n_{z(RBC)} & o_{z(RBC)} & a_{z(RBC)} & p_{z(RBC)} \\
0 & 0 & 0 & 1
\end{bmatrix} \quad (6)
$$

$$
{}^{CoM}T_{LS} = A_7 A_8 A_9 A_{10} A_{11} A_{12} A_{13} =
$$

$$\begin{bmatrix} n_{x(CLS)} & o_{x(CLS)} & a_{x(CLS)} & p_{x(CLS)} \\ n_{y(CLS)} & o_{y(CLS)} & a_{y(CLS)} & p_{y(CLS)} \\ n_{z(CLS)} & o_{z(CLS)} & a_{z(CLS)} & p_{z(CLS)} \\ 0 & 0 & 0 & 1 \end{bmatrix} \tag{7}$$

$${}^{LB}T_{CoM} = A_iA_1A_2A_3A_4A_5A_6A_{CoM} =$$

$$\begin{bmatrix} n_{x(LBC)} & o_{x(LBC)} & a_{x(LBC)} & p_{x(LBC)} \\ n_{y(LBC)} & o_{y(LBC)} & a_{y(LBC)} & p_{y(LBC)} \\ n_{z(LBC)} & o_{z(LBC)} & a_{z(LBC)} & p_{z(LBC)} \\ 0 & 0 & 0 & 1 \end{bmatrix} \tag{8}$$

$${}^{CoM}T_{RS} = A_7A_8A_9A_{10}A_{11}A_{12}A_{13} =$$

$$\begin{bmatrix} n_{x(CRS)} & o_{x(CRS)} & a_{x(CRS)} & p_{x(CRS)} \\ n_{y(CRS)} & o_{y(CRS)} & a_{y(CRS)} & p_{y(CRS)} \\ n_{z(CRS)} & o_{z(CRS)} & a_{z(CRS)} & p_{z(CRS)} \\ 0 & 0 & 0 & 1 \end{bmatrix}. \tag{9}$$

The equations for n, o, a, and p of ${}^{RB}T_{CoM}$ and ${}^{LB}T_{CoM}$ are calculated as shown from (10) to (33), where L_n represents the length of each link $(n = 1, 2, 3, \cdots)$. S_m or C_m are representing $\sin(\theta_m)$ and $\cos(\theta_m)$ respectively $(m = 1, 2, 3, \cdots)$.

$$\begin{aligned} n_{x(RBC)}=&(S_iC_2C_6C_C-S_CC_i)\,C_{(3+4+5)}+\\ &(C_iC_6C_C+S_iS_CC_2)\,S_{(3+4+5)}-S_iS_2S_6C_C \end{aligned} \tag{10}$$

$$\begin{aligned} o_{x(RBC)}=&(S_iC_2C_C-S_CC_iC_6)\,S_{(3+4+5)}-\\ &(S_iS_CC_2C_6+C_iC_C)C_{(3+4+5)}+S_iS_2S_6S_C \end{aligned} \tag{11}$$

$$a_{x(RBC)}=S_iS_6C_2C_{(3+4+5)}+S_6C_iS_{(3+4+5)}+S_iS_2C_6 \tag{12}$$

$$\begin{aligned} n_{y(RBC)}=&(S_iC_6C_C-C_iC_2S_C)\,S_{(3+4+5)}-\\ &(C_iC_2C_6C_C+S_iS_C)\,C_{(3+4+5)}+\\ &C_iS_2S_6C_C \end{aligned} \tag{13}$$

$$\begin{aligned} o_{y(RBC)}=&(S_CC_iC_2C_6-S_iC_C)\,C_{(3+4+5)}-\\ &(S_iC_6S_C+C_iC_2C_C)S_{(3+4+5)}-\\ &S_2S_6S_CC_i \end{aligned} \tag{14}$$

$$\begin{aligned} a_{y(RBC)}=&S_iS_6S_{(3+4+5)}-\\ &C_i(C_2S_6C_{(3+4+5)}+S_2C_6) \end{aligned} \tag{15}$$

$$n_{z(RBC)}=S_2\left(C_6C_CC_{(3+4+5)}+S_CS_{(3+4+5)}\right)+S_6C_2C_C \tag{16}$$

$$o_{z(RBC)}=S_2(C_CS_{(3+4+5)}-S_CC_6C_{(3+4+5)})-S_6S_CC_2 \tag{17}$$

$$a_{z(RBC)}=S_2S_6C_{(3+4+5)}-C_2C_6 \tag{18}$$

$$\begin{aligned} p_{x(RBC)}=&L_7(S_iS_2S_6C_C-(S_iC_2C_6C_C-S_CC_i)C_{(3+4+5)}-\\ &(C_iC_6C_C+S_iS_CC_2)S_{(3+4+5)})+\\ &L_6(S_iS_6C_2C_{(3+4+5)}+C_iS_6S_{(3+4+5)}+S_iS_2C_6)+\\ &L_5(S_iC_2C_{(3+4)}+C_iS_{(3+4)})+\\ &L_4(S_iC_2C_3+C_iS_3)+L_3S_i+L_2C_i \end{aligned} \tag{19}$$

$$\begin{aligned} p_{y(RBC)}=&L_7((C_iC_2C_6C_C+S_iS_C)C_{(3+4+5)}-\\ &(S_iC_6C_C-S_CC_iC_2)S_{(3+4+5)}-C_iS_2S_6C_C)-\\ &L_6(C_iC_2S_6C_{(3+4+5)}-S_iS_6S_{(3+4+5)}+C_iS_2C_6)-\\ &L_5(C_iC_2C_{(3+4)}-S_iS_{(3+4)})-\\ &L_4(C_iC_2C_3-S_iS_3)-L_3C_i+L_2S_i \end{aligned} \tag{20}$$

$$\begin{aligned} p_{z(RBC)}=&-L_7(S_2(C_6C_CC_{(3+4+5)}+S_CS_{(3+4+5)})+\\ &C_2S_6C_C)+L_6(S_2S_6C_{(3+4+5)}-C_2C_6)+\\ &S_2(L_5C_{(3+4)}+L_4C_3) \end{aligned} \tag{21}$$

$$\begin{aligned} n_{x(LBC)}=&(C_iS_C-S_iC_2C_6C_C)C_{(3+4+5)}-\\ &(S_iS_CC_2+C_iC_6C_C)S_{(3+4+5)}+S_iS_2S_6C_C \end{aligned} \tag{22}$$

$$\begin{aligned} o_{x(LBC)}=&(S_iS_CC_2C_6+C_iC_C)C_{(3+4+5)}+\\ &(S_CC_iC_6-S_iC_2C_C)S_{(3+4+5)}-S_iS_2S_6S_C \end{aligned} \tag{23}$$

$$a_{x(LBC)}=S_iS_6C_2C_{(3+4+5)}+S_6C_iS_{(3+4+5)}+S_iS_2C_6 \tag{24}$$

$$\begin{aligned} n_{y(LBC)}=&(C_iC_2C_6C_C+S_iS_C)C_{(3+4+5)}-\\ &(S_iC_6C_C-C_iC_2S_C)S_{(3+4+5)}-C_iS_2S_6C_C \end{aligned} \tag{25}$$

$$\begin{aligned} o_{y(LBC)}=&(S_iC_C-S_CC_iC_2C_6)C_{(3+4+5)}+\\ &(S_iS_CC_6+C_iC_2C_C)S_{(3+4+5)}+S_2S_6S_CC_i \end{aligned} \tag{26}$$

$$a_{y(LBC)}=S_6(S_iS_{(3+4+5)}-C_iC_2C_{(3+4+5)})-S_2C_iC_6 \tag{27}$$

$$\begin{aligned} n_{z(LBC)}=&-S_2\left(C_6C_CC_{(3+4+5)}+S_CS_{(3+4+5)}\right)-\\ &S_6C_2C_C \end{aligned} \tag{28}$$

$$o_{z(LBC)}=S_2(S_CC_6C_{(3+4+5)}-C_CS_{(3+4+5)})+S_6S_CC_2 \tag{29}$$

$$a_{z(LBC)}=S_2S_6C_{(3+4+5)}-C_2C_6 \tag{30}$$

$$\begin{aligned} p_{x(LBC)}=&L_8((S_iC_2C_6C_C-S_CC_i)C_{(3+4+5)}+\\ &(C_iC_6C_C+S_iC_2S_C)S_{(3+4+5)}-S_iS_2S_6C_C)+\\ &L_9(S_iC_2S_6C_{(3+4+5)}+C_iS_6S_{(3+4+5)}+\\ &S_iS_2C_6)-L_{10}(S_iC_2C_{(3+4)}+C_iS_{(3+4)})-\\ &L_{11}(S_iC_2C_3+C_iS_3)-L_{12}S_i+L_{13}C_i \end{aligned} \tag{31}$$

$$\begin{aligned} p_{y(LBC)}=&L_8((S_iC_6C_C-S_CC_iC_2)S_{(3+4+5)}-\\ &(C_iC_2C_6C_C+S_iS_C)C_{(3+4+5)}+S_2S_6C_iC_C)-\\ &L_9(S_6(C_iC_2C_{(3+4+5)}-S_iS_{(3+4+5)})+\\ &S_2C_iC_6)+L_{10}(C_iC_2C_{(3+4)}-S_iS_{(3+4)})+\\ &L_{11}(C_iC_2C_3-S_iS_3)+L_{12}C_i+L_{13}S_i \end{aligned} \tag{32}$$

$$p_{z(LBC)}=L_8(S_2(C_6C_CC_{(3+4+5)}+S_CS_{(3+4+5)})+ C_2S_6C_C)+L_9(S_2S_6C_{(3+4)}-C_2C_6)- S_2(L_{10}C_{(3+4)}+L_{11}C_3). \quad (33)$$

To have these simplified equations, (10) to (33), following trigonometric formulas are used, as shown in (34) and (35).

$$S\theta_1C\theta_2 + C\theta_1S\theta_2 = S(\theta_1+\theta_2) = S_{(1+2)} \quad (34)$$

$$C\theta_1C\theta_2 - S\theta_1S\theta_2 = C(\theta_1+\theta_2) = C_{(1+2)}. \quad (35)$$

To characterize the movements of CoM of the humanoid, a fixed or world reference frame is needed to assign. Fig. 4 shows the fixed reference frame, from where the movement characteristics of CoP and CoM are exemplified.

According to Fig. 4, the 2nd reference frame (R_2) varies on the direction of movement with respect to the 1st reference frame (R_1). The right-toe frame and the left-toe frame are placed at the distance of 3 cm (L_{z_0}=3 cm) from the reference frame R_2. D-H parameters are identified as presented in Table 5. The T matrices from reference frame to toe frame are calculated and presented in (36) and (37). Total transformations from reference frame to CoM, comply with the equations presented in (38) and (39).

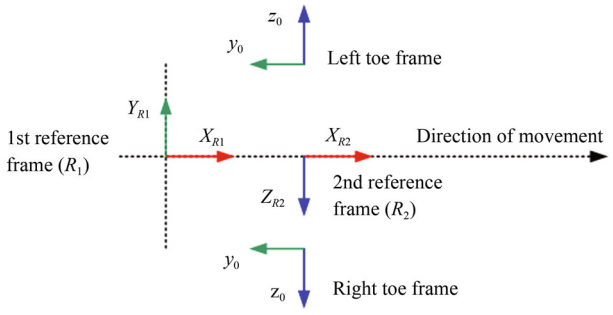

Fig. 4 Assigning the reference frames on the ground (top view)

Table 5 D-H parameters for R_1 to right-toe and left-toe

Joint axes	D-H parameters for reference frame ($^{R1}T_{Rz_0}$ and $^{R1}T_{Lz_0}$)			
	θ_n	d_n	a_n	α_n
A_{R2}	0	0	$a_{R2}=L_{R2}$	$\alpha_{R2}=\frac{\pi}{2}$
A_{Rz_0}	$\theta_{Rz_0}=\frac{\pi}{2}$	$d_{Rz_0}=L_{z_0}$	0	0
A_{Lz_0}	$\theta_{Lz_0}=\frac{\pi}{2}$	$d_{Lz_0}=-L_{z_0}$	0	$\alpha_{Lz_0}=\pi$

$$^{R1}T_{Rz_0}=A_{R2}\times A_{Rz_0}=\begin{bmatrix} 0 & -1 & 0 & L_{R2} \\ 0 & 0 & -1 & -L_{z_0} \\ 1 & 0 & 0 & 0 \\ 0 & 0 & 0 & 1 \end{bmatrix} \quad (36)$$

$$^{R1}T_{Lz_0}=A_{R2}\times A_{Lz_0}=\begin{bmatrix} 0 & 1 & 0 & L_{R2} \\ 0 & 0 & 1 & L_{z_0} \\ 1 & 0 & 0 & 0 \\ 0 & 0 & 0 & 1 \end{bmatrix} \quad (37)$$

$$^{R1}T_{RBC}=^{R1}T_{Rz_0}\,^{RB}T_C \quad (38)$$

$$^{R1}T_{LBC}=^{R1}T_{Lz_0}\,^{LB}T_C. \quad (39)$$

2.4 Walking stability and swing leg planning

For a humanoid system, it is important to maintain the CoM inside the base support area or should move safely inside the base support region if it comes outside of the region. Direction and acceleration of CoM movement of humanoid inverted pendulum is decided by the position of CoP relative to CoM point. Fig. 5 shows the model of quasi inverted pendulum model of humanoid system for lateral movement of walking, where h is the height of CoM from ankle, y_0 is the distance between center line and stance leg tip in coronal plane, l is the length between tip to tip of swing leg in sagittal plane and t is the step time.

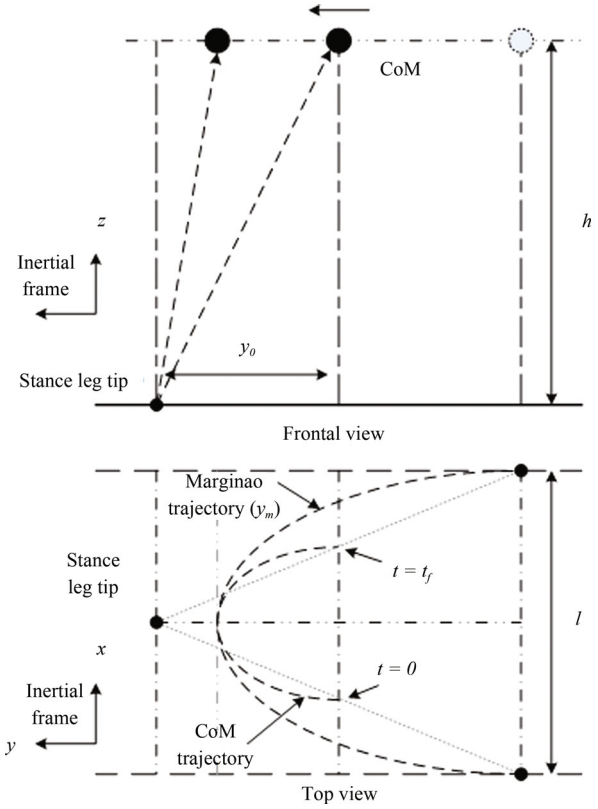

Fig. 5 Quasi inverted pendulum model of humanoid system for lateral walking

The acceleration of CoM varies based on the movement on sagittal and coronal plane which can be defined by (40) and (41), where I_S and I_C are indicating the moment of inertia of the platform about ankle joint in sagittal and coronal plane. CoM_x and CoM_y are presenting forward acceleration and media-lateral (M-L) acceleration of CoM respectively. M is total mass of body, g is the acceleration due to gravity and h is the height of the CoM above ankle joint.

$$\dot{CoM}_x = \frac{Mgh(CoM_x - CoP_x)}{I_S} \tag{40}$$

$$\dot{CoM}_y = \frac{Mgh(CoM_y - CoP_y)}{I_C}. \tag{41}$$

Fig. 6 presents the conceptual design of walking pattern and swing leg planning with ankle joint movement trajectory of the humanoid platform. The pattern is split into three phases, gait initiation (GI), continuous gait (CG), and gait termination (GT). Here x_0 is the tip to tip distance of the swing leg ankle joint and z_0 indicates the height of the swing leg ankle from ground contact.

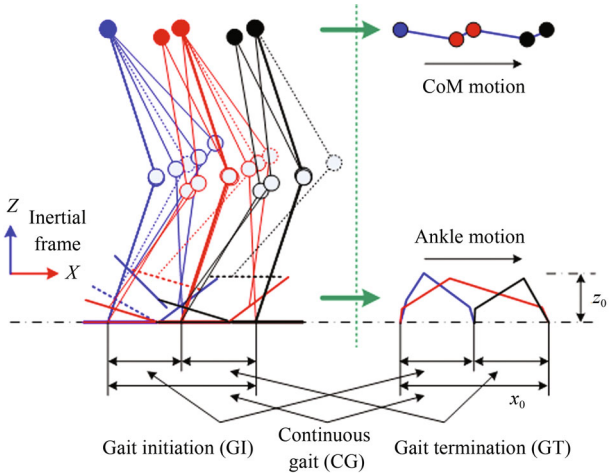

Fig. 6 Walking pattern and ankle joint movements in sagittal plane

Angular velocity, ω, of the humanoid compound pendulum can be calculated based on (42) and (43), where ω_S and ω_C indicate the angular velocity of the humanoid compound pendulum in sagittal and coronal plane. For a stable walking, velocity of ankle should be controlled and the swinging foot must be landed on ground before humanoid becomes unstable.

$$\omega_S = \sqrt{\frac{Mgh}{I_S}} \tag{42}$$

$$\omega_C = \sqrt{\frac{Mgh}{I_C}}. \tag{43}$$

In sagittal plane, CoM motion trajectory should pass the stance point to reflect locomotion. Moreover the CoM trajectory for the lateral movement should not cross over the stance point to ensure a stable walking. The initial condition for CoM point in sagittal plane can be defined by (44) and (45), where $x_0 > 0$ and $v_{x0} > 0$.

$$x_{CoM}(t_0) = -x_0 \tag{44}$$

$$\dot{x}_{CoM}(t_0) = v_{x0}. \tag{45}$$

The initial condition of CoM trajectory in lateral plane can be identified by (46) and (47), where $y_0 > 0$ and $v_{y0} > 0$.

$$y_{CoM}(t_0) = -y_0 \tag{46}$$

$$\dot{y}_{CoM}(t_0) = v_{y0}. \tag{47}$$

The following inequalities presented in (48) are also needed to be considered for a stable walking.

$$v_{x0} > \sqrt{\frac{g}{h}}x_0, \quad v_{y0} < \sqrt{\frac{g}{h}}y_0. \tag{48}$$

For both of the sagittal and coronal planes, CoM trajectory can be described as presented in (49) and (50).

$$x_{CoM}(t) = c_{x1}\mathrm{e}^{-\sqrt{\frac{g}{h}}t} + c_{x2}\mathrm{e}^{\sqrt{\frac{g}{h}}t} \tag{49}$$

$$y_{CoM}(t) = c_{y1}\mathrm{e}^{-\sqrt{\frac{g}{h}}t} + c_{y2}\mathrm{e}^{\sqrt{\frac{g}{h}}t}. \tag{50}$$

Here c_{x1}, c_{x2}, c_{y1} and c_{y2} are defined in (51)−(54).

$$c_{x1} = -\frac{1}{2}\sqrt{\frac{h}{g}}\left(v_{x0} + \sqrt{\frac{g}{h}}x_0\right) \tag{51}$$

$$c_{x2} = \frac{1}{2}\sqrt{\frac{h}{g}}\left(v_{x0} - \sqrt{\frac{g}{h}}x_0\right) \tag{52}$$

$$c_{y1} = -\frac{1}{2}\sqrt{\frac{h}{g}}\left(v_{y0} + \sqrt{\frac{g}{h}}y_0\right) \tag{53}$$

$$c_{y2} = \frac{1}{2}\sqrt{\frac{h}{g}}\left(v_{y0} - \sqrt{\frac{g}{h}}y_0\right). \tag{54}$$

Using the inequality from (48), the above equations can be expressed as, $c_{x1} < 0$, $c_{x2} > 0$, $c_{y1} < 0$ and $c_{y2} > 0$. Now, it is important to select the trajectory of swing leg in such a way that if the swing leg becomes stance position, lateral stability should be maintained. There could be a little difference between the actual step time and the planned step time. For the lateral motion, the desired trajectory of swing leg can be defined as the function of CoM so that the lateral stability of the system is always maintained while switching the stance leg. The swing leg marginal and nominal trajectories in lateral plane are defined by (55) and (56).

$$y_m(t) \overset{\text{def}}{=} y_{CoM}(t) + \sqrt{\frac{h}{g}}\dot{y}_{CoM}(t) = 2c_{y2}\mathrm{e}^{\sqrt{\frac{g}{h}}t} \tag{55}$$

$$y_n(t) \overset{\text{def}}{=} y_{CoM}(t) + \frac{y_0}{v_{y0}}\dot{y}_{CoM}(t). \tag{56}$$

It is possible to adjust the maximum lateral speed by deviating the lateral trajectory from the nominal trajectory of the swing leg. Maximum lateral speed will decrease if the value goes towards the marginal trajectory. The maximum lateral speed will be increased if the value goes away from the marginal trajectory. The total step time is a constant value and can be determined by (57).

$$t_s = \sqrt{\frac{h}{g}}\ln\left(\frac{y_0 + \sqrt{\frac{h}{g}}v_{y0}}{y_0 - \sqrt{\frac{h}{g}}v_{y0}}\right) = \sqrt{\frac{h}{g}}\ln\left(\frac{\frac{y_0}{v_{y0}} + \sqrt{\frac{h}{g}}}{\frac{y_0}{v_{y0}} - \sqrt{\frac{h}{g}}}\right). \tag{57}$$

Based on the above formulation, step time t_s is calculated as 0.969 9 s. ($t_s \approx 1.00$ s). So, the swing leg tip velocity on z direction can be calculated based on equation presented in (58).

$$v_{Swing_z} = \frac{z_0}{t_s} \tag{58}$$

2.5 Inverse kinematic (IK) investigation

To achieve the stable mobility of a humanoid system, it is necessary to have the required position and orientation of each joint so that the CoM point can follow the CoP shifting trajectory. For this project, IK solution is investigated based on geometric-trigonometric approach.

2.5.1 Determining action pose

Action pose is considered as the prelude for any particular action executed by the system. Fig. 7 (a) is representing left view of lower torso of the platform, and Fig. 7 (b) is geometric representation (triangle BAC) of three joints. Knee pitch (θ_{14}), hip pitch (θ_{12}), and ankle pitch (θ_{16}). Objective is to shift the knee pitch, point B, just on the line, AC, where the resulted pose is considered as the action pose of the system. Two lines can be considered, BD and EF, which are perpendicular and parallel with AC. Now, following relations can be established as presented in (59).

$$\begin{cases} AB = BC = L_5 = L_{10} = L_4 = L_{11} \\ BD = d \end{cases} \tag{59}$$

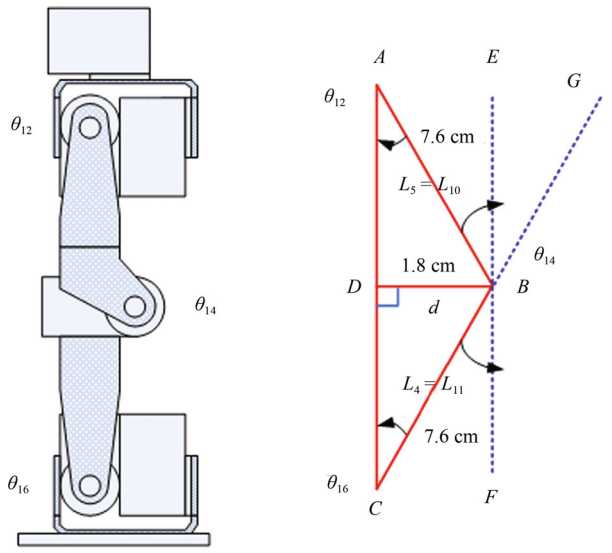

(a) Left view (b) Pitch joint geometry

Fig. 7 Geometric formulation of lower limbs transforming from initial pose to action pose

Applying geometric and trigonometric formulation, desired angular displacement for pitch joints of both legs are possible to establish as presented in (60) to (62).

$$\theta_{11} = \theta_{12} = \sin^{-1}\left(\frac{d}{L_{10}}\right) \tag{60}$$

$$\theta_{13} = \theta_{14} = 2\sin^{-1}\left(\frac{d}{L_{10}}\right) \tag{61}$$

$$\theta_{15} = \theta_{16} = \sin^{-1}\left(\frac{d}{L_{11}}\right). \tag{62}$$

General equation for updating the angular values of each joint is presented in (63), where "±" indicates the clockwise and counter-clockwise direction of the angular movements based on the right hand rule.

$$\theta_{\text{new}} = (\theta_{\text{old}} + (\pm\theta_{\text{calculated}})). \tag{63}$$

2.5.2 Double support phase (DSP) to single support phase (SSP) transformation

To transform phase from DSP to SSP, torso moves sidewise so that CoM point goes closer to the corresponding stance foot which makes the SSP stable. Fig. 8 shows the geometry assigned on coronal plane of lower limbs in finding desired joint angles for DSP to SSP transformation. Necessary conditions are presented in (64)−(66).

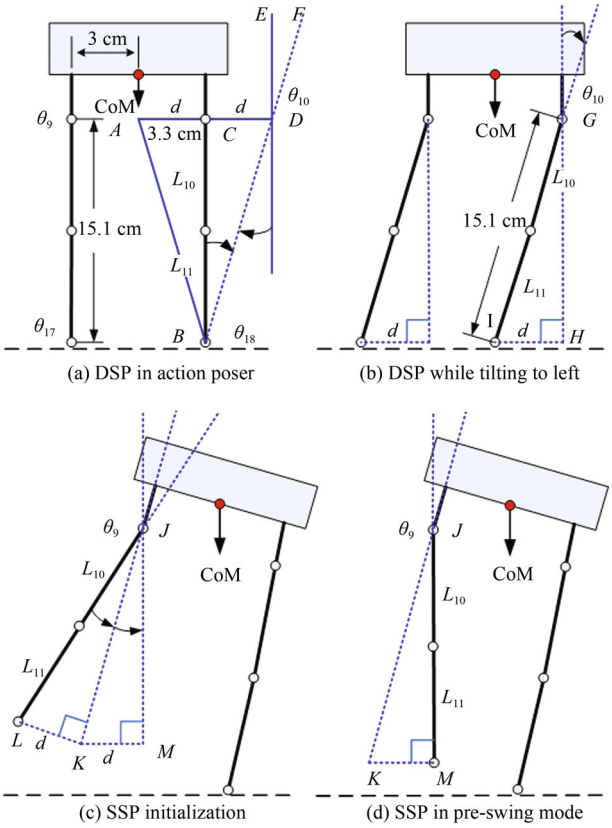

Fig. 8 Geometry of lower limbs transforming DSP to SSP

$$\theta_9 = \theta_{17} = \theta_{10} = \theta_{18} = \tan^{-1}\left(\frac{d}{(L_{10} + L_{11})}\right) \tag{64}$$

$$\theta_{10} = \sin^{-1}\left(\frac{d}{(L_{10} + L_{11})}\right) \tag{65}$$

$$\theta_9 = 2\sin^{-1}\left(\frac{d}{(L_{10} + L_{11})}\right). \tag{66}$$

3 Sensor attachment and center of pressure (CoP) measurement

To identify vertical force induced on ankles of the humanoid, four FSR sensors are attached at the contact surface of each foot. For identification of heel-contact, heel-off, toe-contact, and toe-off moments while performing forward walking, two custom made switches are installed at the heel and toe positions of each foot. Fig. 9 shows the attachment of FSR sensors and contact switches at the plantar surface of each foot. Fig. 10 is presenting a conceptual model in calculating y-components of CoP.

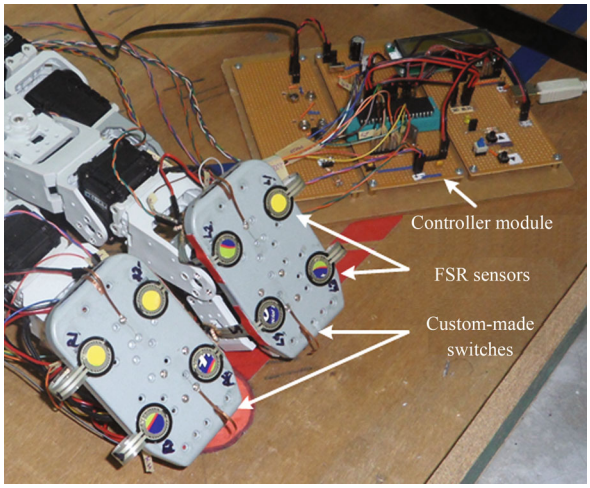

Fig. 9 FSR sensors and contact switches, attached with plantar surface of each foot

According to Fig. 10, y_1 and y_2 are the lateral distance of left and right feet from the center line of walking direction. Total pressure induced on left and right ankles are represented by L_P and R_P which are calculated based on (67) where L_{Pi} and R_{Pi} are the values obtained from each FSR sensor of left and right feet respectively, (i=1,2,3, and 4). Position of CoP will be on the center line if the pressures on both of the ankles are equal.

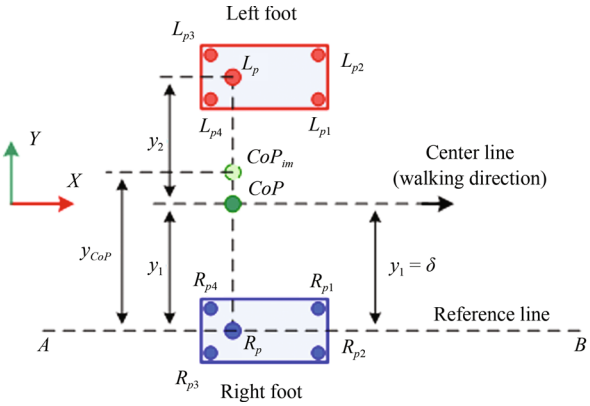

Fig. 10 Modeling the y-component of CoP

$$L_P = \sum_{i=1}^{i=4} L_{Pi} \text{ and } R_P = \sum_{i=1}^{i=4} R_{Pi}. \tag{67}$$

The point, CoP_{im}, is indicating an imaginary position of CoP for a certain condition. Now, considering an imaginary reference line on the right ankle parallel to the center line, y-component of CoP (y_{CoP}) can be calculated based on the equation presented in (68) where δ_y is the adjustment parameter which is equal to the distance between center line and imaginary reference line. The position of CoP with respect to center line can be presented based on the relations shown in (69).

$$y_{CoP} = \left(\frac{L_p\,(y_1 + y_2)}{L_p + R_p}\right) - \delta_y \tag{68}$$

$$\begin{cases} y_{CoP} = 0 & \text{if} \quad L_p = R_p \\ y_{CoP} > 0 & \text{if} \quad L_p > R_p \\ y_{CoP} < 0 & \text{if} \quad L_p < R_p \\ y_{CoP} = y_1 & \text{if} \quad L_p = 0 \\ y_{CoP} = y_2 & \text{if} \quad R_p = 0. \end{cases} \tag{69}$$

Similarly, x-component for CoP can be calculated as presented in (70) where $Lead_p$ is the ankle pressure of leading foot and $Rear_p$ is the ankle pressure of rear foot. Distance of the rear ankle and lead ankle from the center line of x-component (perpendicular to the walking direction) are indicated by x_1 and x_2. The adjustment factor, δ_x, is equal to the distance between center line and imaginary reference line of x-component.

$$x_{CoP} = \left(\frac{Lead_p\,(x_1 + x_2)}{Lead_p + Rear_p}\right) - \delta_x. \tag{70}$$

4 Algorithm design, implementation and result presentation

Block diagram of the designed algorithm for bipedal forward walking is presented in Fig. 11. According to the algorithm, at the initiation stage, CoM trajectory is generated based on QIP model of the biped.

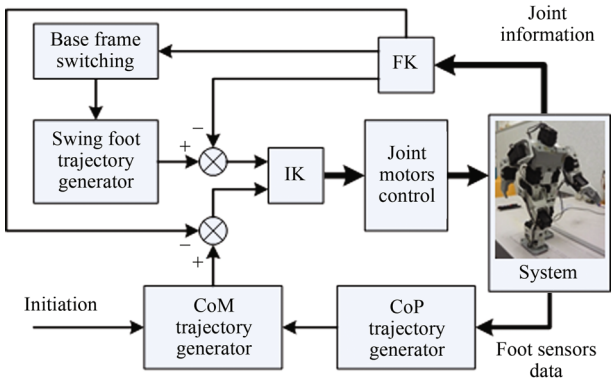

Fig. 11 Block diagram of designed algorithm for bipedal walking

In practical case, CoM trajectory is also guided by the calculated CoP pattern. For an instance, the current position of CoM is calculated in FK block and compared with desired position of generated CoM. The result is fed to IK block to calculate necessary angular changes for each joint

of the kinematic chain. The switching of base frame (stance foot) from ankle to ankle is performed depending on the position of CoM with respect to the center line of walking.

Swing foot trajectory generator produces necessary pattern depending on QIP model of the biped. For the error correction between actual and desired ankle positions, IK block calculates necessary angles of the kinematic chain (CoM to swing foot ankle joint). Depending on the information identified in IK, joint motors controller maintains required movements and velocity to propel the biped with forward walking pattern.

The servo actuators (Dynamixel $AX-12$) are used for each joint that supports $0^\circ - 300^\circ$ as operating angles with maximum holding torque $1.2 \sim 1.6$ N·m. Actuator has onboard ATMega8 μ-controller having 1 MBps speed with half duplex asynchronous serial communication protocol. Each actuator supports serial networking (ID range: $0-253$), and provides position, velocity, load, temperature, and input voltage information as feedback. Using RS485, it is possible to send desired angular position and velocity to the servos.

As the biped is modeled to walk on straight line, the distance of ankles from the center line is considered as 3 cm. and the biped is always trying to maintain this condition. The boundary condition for CoM trajectory is defined as -2.5 cm to 2.5 cm for the lateral movement where the center line is considered as the reference. As the CoM is crossing the centerline while walking, the necessary condition for switching the base frame is presented in (71). Base frame will switch from right to left or left to right, if the y-component of CoM (y_{CoM}) is greater than 0.3 cm or less than -0.3 cm. In between these boundary values (0.3 cm and -0.3 cm), the base frame will maintain its most recent position. Fig. 12 shows the conceptual model of CoM trajectory and base frame shifting moments.

$$\begin{cases} \text{Base frame to Left} & \text{if} \quad y_{CoM} > 0.3\,\text{cm} \\ \text{Base frame to Right} & \text{if} \quad y_{CoM} < -0.3\,\text{cm} \\ \text{Recent position} & \text{if} \quad y_{CoM} \leq 0.3\,\text{cm} \\ & \quad\; y_{CoM} \geq -0.3\,\text{cm}. \end{cases} \tag{71}$$

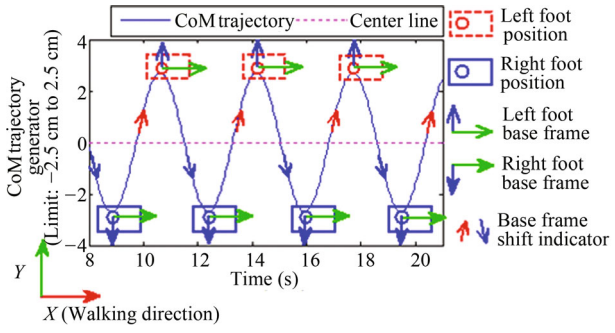

Fig. 12 Generated CoM trajectory pattern and pointing the base frame shifting moment

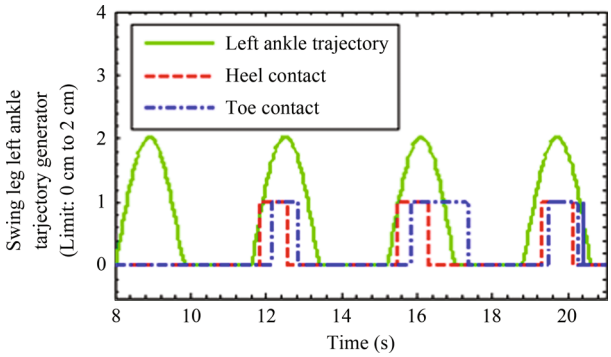

Fig. 13 Designing swing leg ankle trajectory comparing with experimental data of Heel and Toe contact behavior

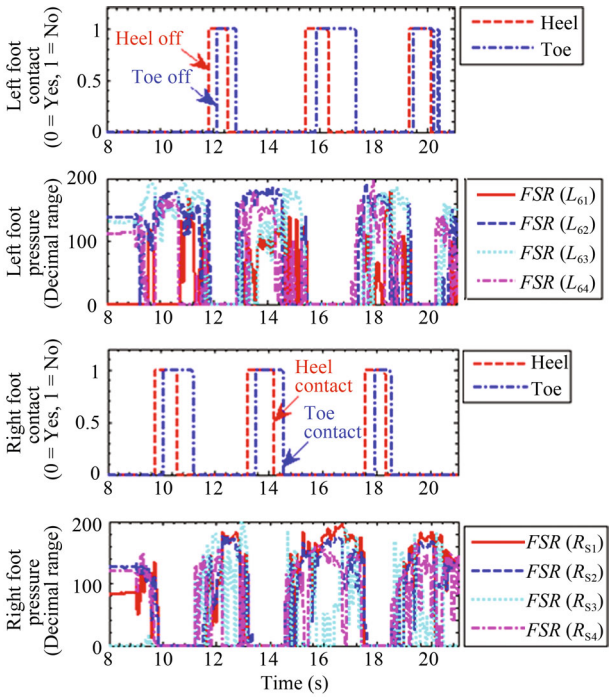

Fig. 14 Pressure induced on individual FSR sensor with heel and toe contact behavior of the biped robot while walking

Swing leg ankle trajectory is designed based on QIP model of the bipedal system as presented in Fig. 13 comparing the experimental result of heel and toe contact behavior pattern of forward walking.

Fig. 14 presents the behavior pattern of pressure induced on each FSR sensor while the bipedal robot is walking forward. Here sensor readings in decimal range are considered instead of actual pressure. The figure also presents heel-contact and toe-off (HC-TO) behavior of the walking pattern which comply with natural walking behavior.

As the custom made switches are used at heel and toe position, the ground reaction forces (GRF) are not considered in designing the bipedal walking. From the behavior pattern of FSR sensors, total induced pressures on left and right ankle are calculated using (67). Behavior pattern of induced pressure on left and right ankles are presented in

Fig. 15 (a). Fig. 15 (b) is presenting the behavior pattern of CoP movement of the bipedal robot while stepping forward.

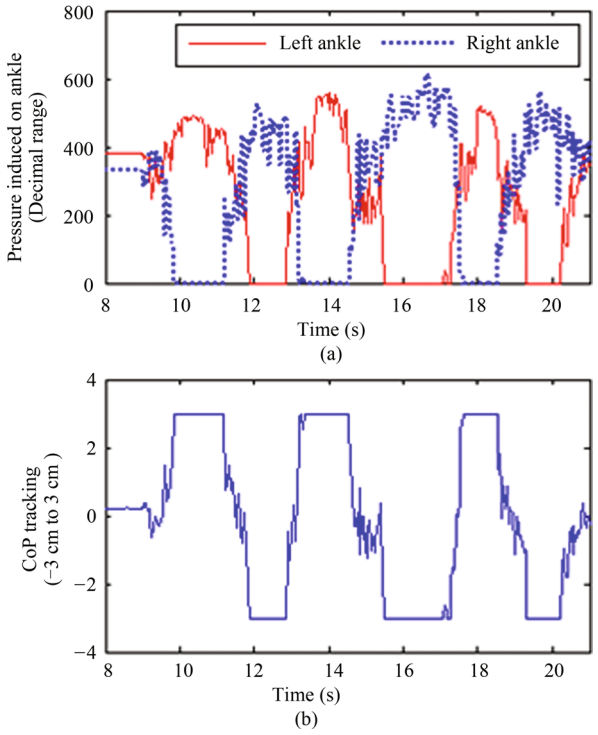

Fig. 15 CoP trajectory pattern based on left and right ankle pressures. (a) Pressure induced on both ankles of biped; (b) Experimental behavior of CoP trajectory for forward walking

Fig. 16 presents experimental behavior pattern of CoM and CoP movements while the biped is walking forward. The figure also compares with the generated CoM movement trajectory. For better understanding of the walking behavior, experimented results are also presented in 3D format as shown in Fig. 17.

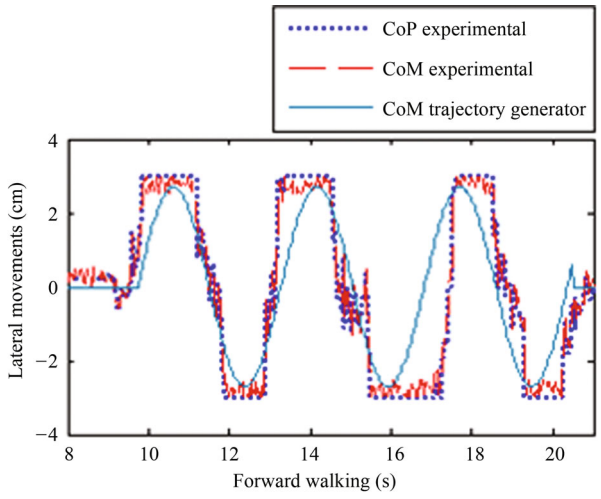

Fig. 16 Experimental results of CoP and CoM motion trajectories while the biped is stepping forward

Experimental results of ankle motion trajectories for both legs are shown in Fig. 18. The figure also illustrates the behavior of heel-off and toe-off moments of SSP when ankle starts to swing. heel-contact and toe-contact moments are indicating the end of SSP as well as the end of ankle swing of a particular leg. At this moment, DSP starts and continues for next heel-off and toe-off moments. Fig. 19 presents the angle variations of each joint actuator associated with lower limbs of the biped while walking three steps forward.

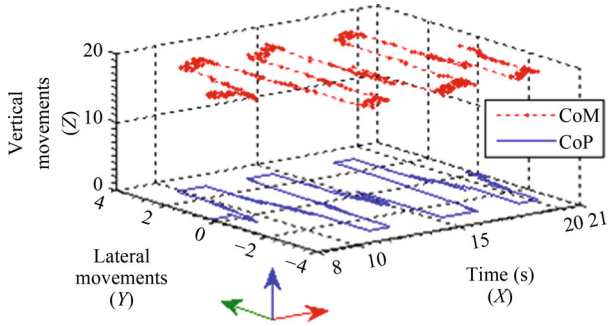

Fig. 17 3D representation of CoP–CoM trajectory patterns of biped forward walking (experimental)

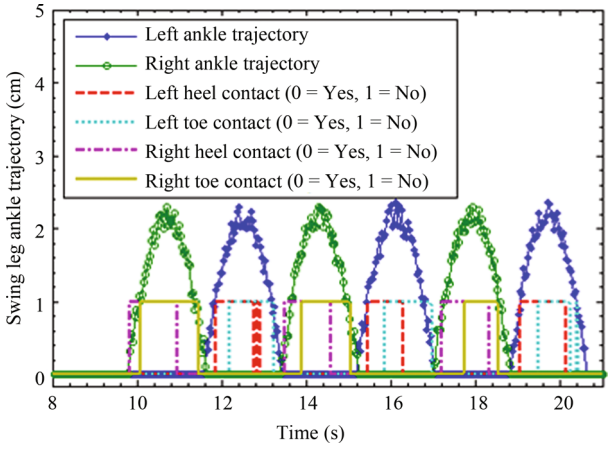

Fig. 18 Experimental results of ankle motion trajectories with heel-contact, heel-off, toe-contact, and toe-off behavior for forward walking of the biped

5 Conclusions

The project is carried out as a M. Sc. program to design and develop a locomotion strategy for a bipedal robot in indoor environment. This paper presents the preliminary stage of the project where a bipedal system is modeled based on QIP modeling technique concentrating on the 12 DoF kinematic chain of the lower limbs of the robot. For this project, two custom made switches are attached at the plantar surface of heel and toe positions to detect heel contact and toe off moment while the biped is performing its forward steps. Four FSR sensors are also attached at the plantar surface of each foot to determine the pressure induced behavior on each of the ankle joints which leads to calculate the CoP with its x and y components. Results of the practical experimentation show that the designed al-

gorithm is viable in balancing the biped while walking forward on straight path. Later the model is used in designing several locomotion strategies, such as, turning, walking on irregular path, obstacle overcoming, and stepping up-down stairs.

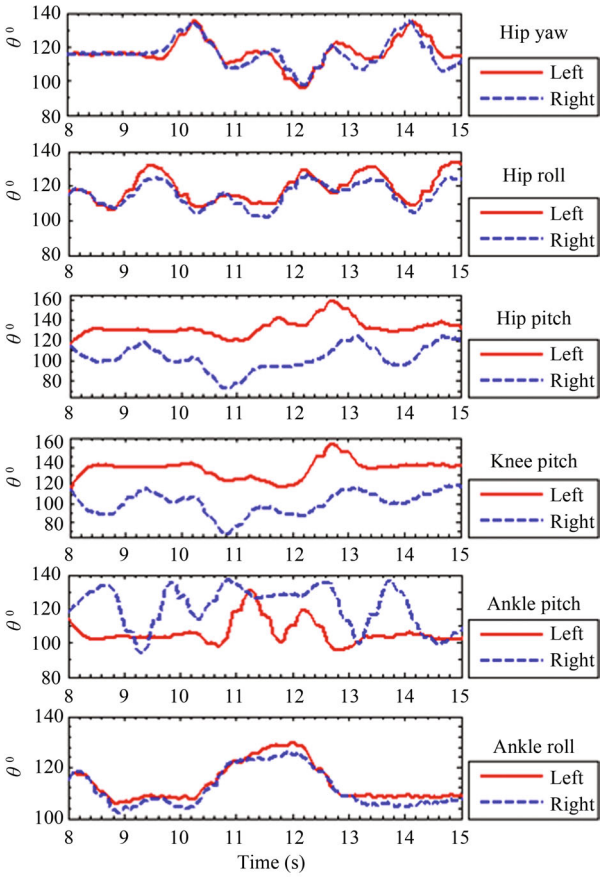

Fig. 19 Experimental data of angle variations of each joint associated with lower limbs of the biped while walking forward

Acknowledgement

Authors would like to express their gratitude to the Ministry of Higher Education (MOHE), Malaysia in funding the project through the MyRA Incentive Grant Scheme (MIRGS), MIRGS 13-02-001-0001.

References

[1] C. Chevallereau, G. Bessonnet, G. Adda, Y. Aoustin. *Bipedal Robots: Modeling, Design and Walking Synthesis*, Hoboken, New Jersey, USA: ISTE Ltd. and John Wiley & Sons, Inc., pp. 1–126, 2008.

[2] Y. Hurmuzlu, F. Génot, B. Brogliato. Modeling, stability and control of biped robots-a general framework. *Automatica*, vol. 40, no. 10, pp. 1647–1664, 2004.

[3] S. B. Niku. *Introduction to Robotics: Analysis, Systems, Applications*, Upper Saddle River, New Jersey, USA: Prentice Hall, Inc., pp. 29–85, 2001.

[4] N. T. Phuong, D. W. Kim, H. K. Kim, S. B. Kim. An optimal control method for biped robot with stable walking gait. In *Proceedings of the 8th IEEE-RAS International Conference on Humanoid Robots*, IEEE, Daejeon, Korea, pp. 211–218, 2008.

[5] P. Gibbons, M. Mason, A. Vicente, G. Bugmann, P. Culverhouse. Optimization of dynamic gait for bipedal robots. In *Proceedings of IEEE-RAS International Conference on Humanoid Robots*, IEEE, Paris, France, pp. 9–14, 2009.

[6] M. Eaton. Further explorations in evolutionary humanoid robotics. In *Proceedings of the 12th International Symposium on Artificial Life and Robotics*, ISAROB, Oita, Japan, pp. 133–137, 2007.

[7] C. Sander, T. Soworka, A. Albers. Design of a new torso-joint for the humanoid robot ARMAR. *Journal of Mechanical Engineering and Automation*, vol. 2, no. 4, pp. 58–64, 2012.

[8] M. Hofmann, I. Schwarz, O. Urbann, E. Erdmann, B. Bohm, Y. Struszczynski. Team Description for RoboCup 2013, Technical Report, TU Dortmund University, Germany, 2013.

[9] D. Gouaillier, V. Hugel, P. Blazevic. Mechatronic design of NAO humanoid. In *Proceedings of IEEE International Conference on Robotics and Automation*, Kobe International Conference Center, Kobe, Japan, pp. 769–774, 2009.

[10] N. Kofinas. Forward and Inverse Kinematics for the NAO Humanoid Robot, Diploma Thesis, Technical University of Crete, Greece, 2012.

[11] R. C. Limón, J. M. I. Zannatha, M. Á. A. Rodríguez. Inverse kinematics of a humanoid robot with non-spherical hip: A hybrid algorithm approach. *International Journal of Advanced Robotic Systems*, vol. 10, pp. 1–13, 2013.

[12] G. S. Toscano, H. Simas, E. D. B. Castelan. Trajectory generation for a spatial humanoid robots using Assur virtual chains through screw theory. In *Proceedings of the 22nd International Congress of Mechanical Engineering*, COBEM, Ribeirão Preto, Brazil, pp. 2727–2738, 2013.

[13] J. de Lope, T. Zarraonandia, R. González-Careaga, D. Maravall. Solving the inverse kinematics in humanoid robots: A neural approach. In *Proceedings of the 7th International Work-conference on Artificial and Natural Neural Networks, Lecture Notes in Computer Science*, Springer, Menorca, Spain, vol. 2687, pp. 177–184, 2003.

[14] M. Zorjan, V. Hugel. Generalized humanoid leg inverse kinematics to deal with singularities. In *Proceedings of IEEE International Conference on Robotics and Automation*, IEEE, Karlsruhe, Germany, pp. 4791–4796, 2013.

[15] J. M. I. Zannatha, R. C. Limón. Forward and inverse kinematics for a small-sized humanoid robot. In *Proceedings of International Conference on Electrical, Communications, and Computers*, IEEE, Cholula, Puebla, pp. 111–118, 2009.

[16] H. S. Jo, N. Mir-Nasiri. Development of minimalist bipedal walking robot with flexible ankle and split-mass balancing systems. *International Journal of Automation and Computing*, vol. 10, no. 5, pp. 425–437, 2013.

[17] M. Akhtaruzzaman, A. A. Shafie. Evolution of humanoid robot and contribution of various countries in advancing the research and development of the platform. In *Proceedings of International Conference on Control, Automation and Systems*, IEEE, Gyeonggi-do, Korea, pp. 1021–1028, 2010.

[18] M. Akhtaruzzaman, A. A. Shafie. Advancement of android and contribution of various countries in the research and development of the humanoid platform. *International Journal of Robotics and Automation*, vol. 1, no. 2, pp. 43–57, 2010.

[19] M. Akhtaruzzaman, A. A. Shafie. A novel gait for toddler biped and its control using PIC 16F877A. In *Proceedings of the 4th International Conference on Mechatronics*, IEEE, Kuala Lumpur, Malaysia, pp. 1–6, 2011.

[20] M. Akhtaruzzaman, A. A. Shafie. An attempt to develop a biped intelligent machine BIM-UIA. In *Proceedings of the 4th International Conference on Mechatronics*, IEEE, Kuala Lumpur, Malaysia, pp. 1–7, 2011.

[21] M. Akhtaruzzaman, A. A. Shafie. Geometrical analysis on BIOLOID humanoid system standing on single Leg, In *Proceedings of the 4th International Conference on Mechatronics*, IEEE, Kuala Lumpur, Malaysia, pp. 1–5, 2011.

[22] M. Akhtaruzzaman, A. A. Shafie, M. Rashid. Component selection strategy for an anthropomorphic robot. In *Proceedings of National Postgraduate Conference*, IEEE, Kuala Lumpur, Malaysia, pp. 1–6, 2011.

[23] M. Akhtaruzzaman, A. A. Shafie, T. Ahsan, M. S. Alam, S. M. Raihan, M. K. Hasan, M. B. Haider. Golden ratio, the Phi, and its geometrical substantiation. In *Proceedings of IEEE Student Conference on Research and Development*, IEEE, Cyberjaya, Malaysia, pp. 425–430, 2011.

[24] M. Akhtaruzzaman, A. A. Shafie. Geometrical substantiation of Phi, the golden ratio and the baroque of nature, architecture, design and engineering. *International Journal of Arts, Scientific & Academic Publishing*, vol. 1, no. 1, pp. 1–22, 2011.

[25] M. Akhtaruzzaman, A. A. Shafie, M. Rashid. Designing an algorithm for bioloid humanoid navigating in its indoor environment. *Journal of Mechanical Engineering and Automation*, vol. 2, no. 3, pp. 36–44, 2012.

[26] D. A. Winter. *Biomechanics and Motor Control of Human Movement*, 4th ed., Hoboken, USA: John Wiley & Sons, Inc., 2009.

M. Akhtaruzzaman received the B. Sc. degree in computer science and engineering (CSE) from International Islamic University Chittagong (IIUC), Bangladesh in 2005. He received the M. Sc. degree in mechatronics engineering (MCT) from Engineering, International Islamic University Malaysia (IIUM), Malaysia in 2012. He is a Ph. D. degree candidate in mechatronics engineering, Kulliyyah of IIUM, Malaysia. He has published several papers in the area of modeling and control, robotics, and mechatronics system design.

His research interests include modeling and control of mechatronics systems, biped robot, and rehabilitation engineering.

E-mail: akhter900@gmail.com (Corresponding author)
ORCID iD: 0000-0002-9929-4066

Amir A. Shafie received the B. Eng. degree (Hons) in mechanical engineering from the University of Dundee, UK, and M. Sc. degree in mechatronics from University of Abertay Dundee, UK. He has been conferred a doctorate in the field of artificial intelligence by University of Dundee, UK in 2000. He is currently attached to International Islamic University Malaysia as a professor after serving in industry as industrial researcher. He has been principal researcher for various research projects mainly in the area of autonomous mechatronic system which aims to develop intelligent robotic system for industrial and other applications.

His research interests include machine control, biologically-inspired robot, surveillance system, image processing and computer vision.

E-mail: aashafie@iium.edu.my

Md. Raisuddin Khan received the B. Sc. degree in mechanical engineering from Rajshahi University of Engineering and Technology (RUET), Bangladesh in 1983, and received the M. Sc. degree in mechanical engineering from the same University, in 1988. He received the Ph. D. degree in mechanical engineering from Bangladesh University of Engineering and Technology (BUET), Bangladesh in 1996. He is currently attached with International Islamic University Malaysia as a professor. He has a prominent number of publications including journals, books, book chapters, and conferences. He was also awarded several national and international awards as the recognition of his remarkable works.

His research interests include bio-inspired robot, robot assistive systems, vibration, stress, and stability of structure.

E-mail: raisuddin@iium.edu.my